

Interplay between the Hawking effect and the quasi-normal modes of a one-dimensional sonic horizon in a polariton fluid

M. Joly¹, L. Giacomelli², F. Claude¹, E. Giacobino¹, Q. Glorieux¹, I. Carusotto², A. Bramati¹, and M. J. Jacquet^{1*}

¹ *Laboratoire Kastler Brossel,
Sorbonne Université, CNRS, ENS-Université PSL,
Collège de France, Paris 75005, France*

² *INO-CNR BEC Center and Dipartimento di Fisica,
Università di Trento, via Sommarive 14,
I-38050 Povo, Trento, Italy*

* *correspondance to maxime.jacquet@lkb.upmc.fr*

Analogue gravity enables the laboratory study of the Hawking effect, correlated emission at the horizon. Here, we use a quantum fluid of polaritons as a setup to study the statistics of correlated emission. Dissipation in the system may quench quasi-normal modes of the horizon, thus modifying the horizon structure. We numerically compute the spectrum of spatial correlations and find a regime in which the emission is strongly enhanced while being modulated by the quasi-normal modes. The high signal-to-noise ratio we obtain makes the experimental observation of these effects possible, thus enabling the quantitative study of the influence of dissipation and of higher order corrections to the curvature on quantum emission.

Quantum fluctuations at the event horizon of black holes cause the emission of correlated waves by the Hawking effect (HE) [1]: while some waves (Hawking radiation) propagate away from the horizon to outer space, others (the partner radiation) fall inside the horizon. Since signaling from inside the horizon is impossible, only Hawking radiation may be detected and correlations between paired waves cannot be measured in astrophysics. The HE may also be observed in the laboratory thanks to analogue gravity setups [2, 3]. These are media whose properties may be engineered such that waves within propagate on effectively curved spacetimes [4, 5], as has been experimentally demonstrated in a variety of platforms [6–17]. For example, there is a horizon for sound waves in a one-dimensional transsonic fluid where the flow velocity of the fluid equals the speed of sound. The HE at the sonic horizon yields the emission of correlated waves just like in astrophysics [4, 5], with the notable difference that observation on both sides of the horizon is possible.

Experimental evidence for correlated emission at horizons was recently reported in analogue gravity setups based on classical [18] and quantum fluids [19]. While the thermal fluctuations of classical fluids overpower quantum fluctuations at the horizon such that spontaneous emission cannot be observed there, this can be done with quantum fluids. Spontaneous emission would yield a non-separable state at the output [20–29], whose degree of entanglement could be quantified from the density and correlation spectra [30, 31].

Although most work on spontaneous emission has been dedicated to atomic Bose-Einstein condensate (BEC) analogues [32–40], correlated emission with comparable properties may also be observed in quantum fluids of microcavity exciton-polaritons (polaritons) where a sonic horizon has already been experimentally realised in one- and two-dimensional microcavities [11, 41]. In both quantum fluids, the Hawking effect manifests itself as the emission of so-called Bogoliubov excitations (elementary excitations of the fluid whose kinematics are ruled by its dispersion) that propagate in opposite directions on either side of the horizon.

In this paper, we explore the parameter space of quantum

fluids of polaritons to find a regime favourable to the formation of correlations by the HE. The hydrodynamics of the fluid are controlled by its density and phase, which are in turn connected with the optical bistability of the system (the hysteresis cycle of its polariton-density-to-optical-power relationship), and so we investigate spontaneous emission from this perspective. We study the influence of the regime of bistability on either side of the horizon on the properties of emission by the Hawking effect. In doing so, we also find that, besides yielding correlated emission by the HE, quantum vacuum fluctuations also perturb the horizon that rings down. This linear response of the perturbed horizon is understood in terms of damped resonances called quasinormal modes (QNMs) [42–44]. These are complex frequency modes whose real and imaginary parts correspond to their oscillation frequency and lifetime, respectively. To date, QNMs have only been observed in two-dimensional rotating flows [45]. They have also been studied in the context of large amplitude perturbations destabilising the horizon and the so-called black-hole laser in one-dimensional conservative quantum fluids [46–49], but it is the first time they are observed in a driven-dissipative fluid. Here we show that dissipation quenches these modes which form atmospheres (higher order corrections to the curvature of the effective spacetime) on either side of the horizon, thus modulating correlated emission by the HE. Fine control upon the regime of bistability provides us with a better understanding of the influence of the properties of the quantum fluid of polaritons on the propagation of Bogoliubov excitations as well as on emission by the HE therein. Our results open the way to the experimental observation of spontaneous emission from the vacuum in polaritonic systems and to further study of fluctuation-driven instabilities of sonic horizons.

Sonic horizon in a polariton fluid Our study is based on the experiment [11]: the physical device is a GaAs microcavity sandwiched between a pair of planar Bragg reflectors with alternating $\lambda/4$ layers of GaAs/AlGaAs. An InGaAs quantum well is inserted in the microcavity layer, whose thickness is chosen so that the cavity mode is resonant with the quantum well excitonic transition to obtain polaritons. The micro-

cavity is elongated over $500\text{ }\mu\text{m}$ in one direction and kept to a constant transverse width of $3\text{ }\mu\text{m}$ to form a wire in which the polariton dynamics are effectively one-dimensional. As in [11, 50, 51], we pump the microcavity with a continuous wave, coherent pump laser incident at a given angle with respect to the normal to form a stationary flow along the wire. However, instead of using a Gaussian spatial mode, we structure the light field to pump with a step-like intensity profile. In the region where the pump lies, the density and phase properties of the polariton fluid are set by those of the pump, while in the region where the pump intensity is zero, polaritons propagate ballistically. As in [11, 51, 52], we consider a cavity with an attractive defect (a localised $1\text{ }\mu\text{m}$ long broadening of the wire to a width of $5.6\text{ }\mu\text{m}$) placed downstream of the region where the pump lies. The defect at $x = 0$ will create a dip in the fluid density and a spike in the flow velocity because of the conservation of the flow current. The density profile of the polariton fluid $\sqrt{\hbar g n/m}$ ($\hbar g$ the interaction energy, n the mean-field density of polaritons, m their effective mass) is shown in blue in Fig. 1 (c) in laboratory frame coordinates x and t . We see that the polariton density is almost flat before the defect and decreases afterwards. The polariton dynamics are driven-dissipative: polaritons have a lifetime γ after which they de-excite, releasing a photon that leaks out of the cavity, enabling the direct monitoring of the density and phase of the fluid.

In Appendix A, we review the theory for polariton hydrodynamics in a homogeneous system as described by a modified Gross-Pitaevskii equation (GPE). There we show how the polaritons behave as a fluid and describe the dispersive properties of elementary (or Bogoliubov) excitations therein. These depend on the effective detuning between the pump energy $\hbar\omega_p$ and that of polaritons $\hbar\omega_0$, $\Delta_p = \omega_p - \omega_0 - \frac{\hbar k_p^2}{2m}$, where k_p is the wavenumber of the pump field. In the case $\omega_p > \omega_0$ ($\Delta_p > \gamma\sqrt{3}/2$), the steady-state GPE is

$$\left[(gn - \Delta_p)^2 + \frac{\gamma^2}{4} \right] n = |F_p|^2, \quad (1)$$

with F_p the laser field. The equation of state (1) describes the bistable behaviour of the fluid [53]: as shown in Fig. 1 (a), there is a hysteresis relationship between gn and $|F_p|^2$, which we will henceforth refer to as the ‘bistability loop’.

The kinematics of Bogoliubov excitations of the fluid are governed by the dispersion relation. In Appendix A, we calculate and study the properties of the dispersion relation as a function of Δ_p in the frame co-moving with the fluid at velocity $v = \frac{\hbar}{m}\partial_x\theta$. Here we write the dispersion relation ω_{\pm}^L in the laboratory frame (where measurements are made) by means of a Galilean transform ($\omega^L \rightarrow \omega v \delta k$, with $\delta k = k - k_p$):

$$\omega_{\pm}^L(k) = \pm \sqrt{\left(\Delta_p - \frac{\hbar \delta k^2}{2m} - 3gn \right) \left(\Delta_p - \frac{\hbar \delta k^2}{2m} - gn \right)} + v \delta k - i\gamma/2. \quad (2)$$

The dispersion relation (2) depends on both the density n and the velocity of flow v of the fluid [54].

The case of interest is that of a transsonic fluid flow, that is a flow which goes from being sub- to supersonic with a sonic horizon ($v = c_s$) at $x = 0$ [55]. This is the canonical ‘waterfall configuration’ of the transsonic flow studied in the analogue gravity literature with quantum fluids. The waterfall is composed of two homogeneous regions of different density (and hence speed of sound) and phase (and hence flow velocity). The region where the flow is subsonic is *upstream* of, or *outside*, the horizon. The region where the flow is supersonic is *downstream* of, or *inside*, the horizon.

In Fig. 1, we plot the dispersion relation (2) of the inhomogeneous fluid in the laboratory frame for two different pumping strengths when pumping at point C of the bistability loop. Blue (orange) curves correspond to positive (negative) energy solutions of Eq. (A10) in the frame co-moving with the fluid. As usual in field theories in analogue gravity, the modes with positive (negative) energies in the rest frame of the fluid have positive (negative) Klein-Gordon norm [56]. For subsonic fluid flows, the negative norm branch is at negative laboratory frame energies, while for supersonic flows, part of the negative norm branch is pulled up to positive laboratory frame energies by the Doppler effect, up to a maximum energy which we denote by ω_{max} .

Now that we have described the dispersive properties of the inhomogeneous fluid, we consider the kinematics of Bogoliubov excitations therein. Because of the time invariance of the system, these are plane wave modes. Eq. (2) is a fourth-order polynomial, so there are four (positive laboratory-frame frequency) solutions to the equations of motion in each spatial region on either side of the interface. These solutions are found at the intersection point of an $\omega_0 = cst$ line with the dispersion branches at positive energies in Fig. 1. Although these solutions share the same ω (which manifests energy conservation in the laboratory frame), they have distinct k , i.e. they are local modes of the homogeneous system. For $\omega > 0$ in the upstream region there are two propagating modes of positive norm and two modes of complex ω and k , which are exponentially growing and decaying modes. For $\omega < \omega_{max}$ in the downstream region, there are four propagating modes, two of which have positive norm while the other two have negative norm. For $\omega > \omega_{max}$, there are two propagating modes of positive norm and two exponentially growing and decaying modes. The interface at $x = 0$ is a sonic horizon only at frequencies for which there are two propagating local modes in the upstream region and four propagating local modes (including negative-norm modes) in the downstream region [35, 56, 57], i.e., for $\omega \in [0, \omega_{max}]$. In Appendix A 4 we explain how to construct the ‘global modes’ (GMs) of the inhomogeneous system (including the waterfall).

Before moving on to the calculation of spontaneous emission at the horizon, we remark that, in reality, the media on either side of the interface are not strictly homogeneous. Instead their density and phase vary in space. Nevertheless, if the amplitude of these variations is small, the description of the system as two media remains valid, only one has to calculate the dispersion and bistability at all points. However, this renders an analytical calculation overly lengthy (if at all possible), unlike in [35, 56, 57]. So, instead of calculating the

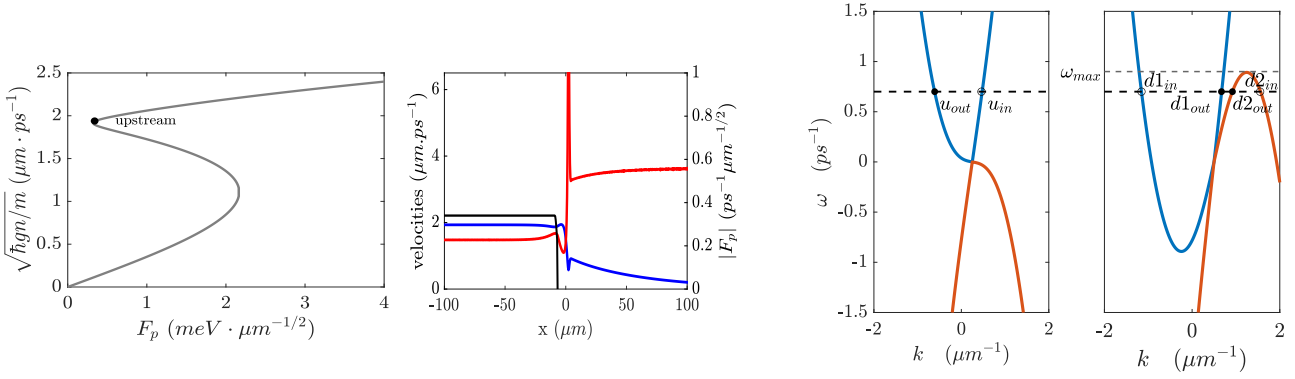


Figure 1. **Properties of a transsonic polariton fluid flow.** (a) bistability loop obtained from Eq. (1). (b) fluid properties when supporting the fluid density and phase in the upstream region at point C of the bistability loop. Black, pump intensity; red, fluid velocity; blue, $\sqrt{\hbar g n}/m$. (c) corresponding Bogoliubov dispersion relation of the inhomogeneous fluid in the laboratory frame. Left (right) column, dispersion relation (2) for a subsonic (supersonic) fluid flow. Blue, positive-norm branch; orange, negative-norm branch. Circles, local modes of positive group velocity; filled dots, local modes of negative group velocity. Dot-dashed line, ω_{max} ; dashed line ω_0 .

scattering matrix analytically, we use the Truncated Wigner Approximation (see Appendix B) to evolve the wave function and obtain the properties of the fluid at all points in the cavity as well as the dynamics of the Bogoliubov excitations therein.

Enhanced Hawking effect We now perform simulations with the cavity parameters of [11]: $\hbar\gamma = 0.047 \text{ meV}$, $\hbar g = 0.005 \text{ meV}\mu\text{m}$, $m = 3 \cdot 10^{-5} m_e$. In Appendix C, we study a variety of configurations of pump spatial profile, wavenumber and intensity and we observe the influence of the regime of density of the fluid (optical bistability) on spontaneous emission at the horizon and propagation in either region thereafter. In doing so, we can explain that the configurations [11, 51, 52] limit the emission of Bogoliubov excitations because of operation with inhomogeneous profiles far from the sonic point of the bistability loop in the upstream region. In Fig. 2, we show the two-point correlations $g^{(2)}(x, x') - 1$ for the optimal configuration, which is when the density and phase of the fluid in the upstream region are homogeneously supported in the bistable regime, specifically at point C in Fig. 1 (a). In all configurations, correlations may be sorted by the region in which the involved modes propagate, which correspond to four quadrants in the plots. The South West quadrant ($x < 0$, $x' < 0$) corresponds to correlations in the upstream region; the South East and North West quadrants correspond to correlations across the horizon in the up- and downstream regions; the North East quadrant corresponds to correlations in the downstream region. All configurations have some common features, which are evident in Fig. 2:

- Anti-correlations along the $x = x'$ diagonal — self correlations of the fluid.
- A negative correlation trace in the *upstream-downstream* region corresponding to $u_{out} - d2_{out}$ correlations, the so-called ‘Hawking moustache’.
- A positive correlation trace in the *upstream-downstream* region corresponding to $u_{out} - d1_{out}$ correlations.
- A positive correlation trace in the *downstream-downstream* region corresponding to $d1_{out} - d2_{out}$ correlations.

- Fringes, both in the *upstream-downstream* region and in the *downstream-downstream* region. See Appendix E
- Strictly horizontal ($x' = 0$) and strictly vertical ($x = 0$) fringes. These have not been observed before.

Except for the last item, these are all generic features of the Hawking effect in dispersive quantum fluids, see eg [32, 40, 51, 52, 56, 58].

In the configuration of Fig. 2, the fluid density is supported near the sonic point in the upstream region, with $k_{p,u} = 0.25 \mu\text{m}^{-1}$, up until $10 \mu\text{m}$ before the horizon, where the strength of the pump drops to zero. Thereafter, the fluid is left to evolve ballistically across the horizon into the downstream region. The Hawking moustache is of amplitude $7.5 \cdot 10^{-4}$ and is about $35 \mu\text{m}$ - and $105 \mu\text{m}$ -long in the up- and downstream regions, respectively. The $u_{out} - d1_{out}$ correlations are of amplitude $2.5 \cdot 10^{-4}$ and the trace is $25 \mu\text{m}$ and $105 \mu\text{m}$ long in the up- and downstream regions, respectively. At long distances, both up-downstream correlation traces become dispersive. The $d1_{out} - d2_{out}$ correlations are of amplitude $6 \cdot 10^{-4}$ and the trace is $110 \mu\text{m}$ long.

Fig. 2 resembles the configuration [52], where the pump was also structured to obtain a flat fluid density in the nonlinear-bistable density regime. In [52], just like in all other configurations considered in Appendix C, there is no effective cavity between the edge of the pump and the horizon (unlike in [11, 51]). Yet, unlike in Fig. 2, the Hawking moustache is short, with a total length of about $25 \mu\text{m}$ whereas we obtain a total length of over $110 \mu\text{m}$. We note that we obtain similar downstream-downstream correlation patterns to [52], so the difference does not lie in the physics in that region. In fact, the fluid accumulates before the horizon: as can be seen in Fig. 2, there is a small but non-negligible bump of width about $7 \mu\text{m}$ in the fluid density just before the horizon. If, as in [52] the fluid density is already at or above the sonic point before that bump, then the density rises such that it is far in the non-linear regime just before the horizon. In contrast, in Fig. 2 the density is supported at the sonic point in the upstream region, and the pump stops $10 \mu\text{m}$ before the horizon such that the accumulation of fluid brings the fluid density

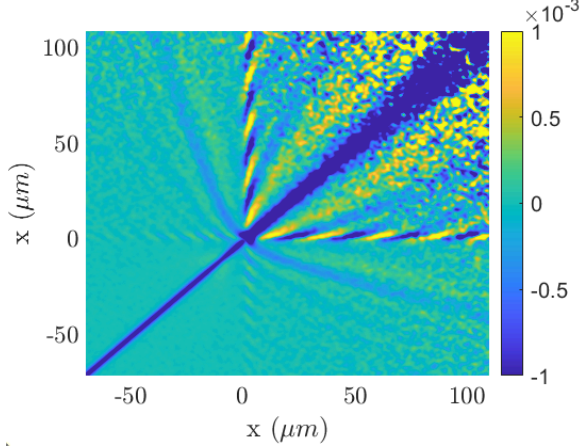


Figure 2. Spatial correlations $g^{(2)}(x, x') - 1$ in the quantum fluid.

on the bump at the sonic point as well. Given the enhanced trace length compared with [52], we postulate that operating at the sonic point upstream of the horizon enhances the propagation of Bogoliubov excitations in that region. We confirm this in Appendix D, where we study the influence of the fluid properties near the horizon on spontaneous emission: we find that Bogoliubov excitations are emitted in the upstream region as long as the fluid density is supported on the upper branch of the bistability loop in the vicinity of the horizon. We also demonstrate that operating at exactly the sonic point there strongly enhances spontaneous emission and, in turn, propagation in the upstream region.

Hawking radiation and quasinormal modes We now turn to the new interference patterns observed in Fig. 2. Since these features develop strictly horizontally and vertically, they correspond to correlations between a propagating mode with a mode whose group velocity is zero. Whence these features signal the excitation of a mode localised near the horizon. The parts of the horizontal and vertical features that go from $x = 0$ towards $x < 0$ and $x' < 0$ are correlations between the localised mode and the Hawking radiation (u_{out}) in the upstream region, while the parts that go towards $x > 0$ and $x' > 0$ are correlations of the same localised mode with the partner wave ($d2_{out}$) in the downstream region. So the localised mode resonates with outgoing Bogoliubov excitations: it is a long-lived trapped mode that couples to a propagating mode, *i.e.*, a quasi-bound state of the horizon [43]. These are predicted to occur in particular for massive fields around Kerr and Schwarzschild black holes [59–61].

We have verified that the fluid density barely evolves within 2γ before the steady-state is reached, meaning that we do operate in the linear regime of interactions. This implies that these localised modes may only be populated by quantum fluctuations of the vacuum that perturb the horizon in addition to generating correlated waves by the Hawking effect. The ringdown frequency of the horizon is obtained by reading out the wavenumber of propagating modes that res-

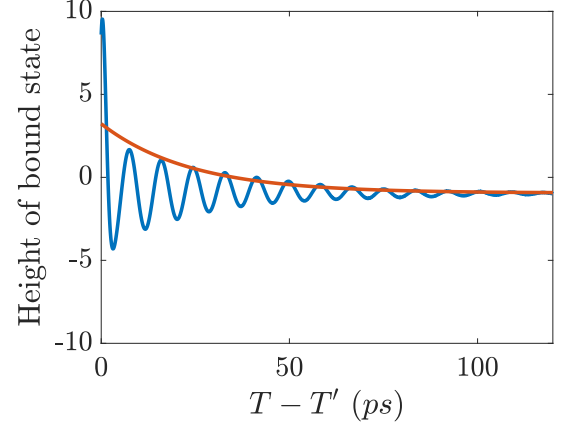


Figure 3. **Relaxation of the horizon.** Blue, peak height of the state bound to the horizon in time after the impact of the wavepacket on the horizon. Orange, exponential fit.

onate with the quasi-bound state on either side of the horizon, $k_u = -0.645 \mu\text{m}^{-1}$ and $k_{d2} = 0.985 \mu\text{m}^{-1}$. These share a frequency $\omega = \text{Re}(\omega_i^Q) = 0.7697 \text{ ps}^{-1}$. In Fig. 3, we show the result of the excitation of the horizon by an incoming wave packet: instead of letting solely the vacuum impinge on the horizon, we send in an additional, small amplitude wave packet (a classical coherent wave) of frequency $\text{Re}(\omega_i^Q)$ coming from the upstream region. We observe the relaxation of the horizon, that is the evolution of the density at the horizon as a function of time and we see that it oscillates with frequency $\text{Re}(\omega_i^Q)$ while damping down exponentially. This damping is a measure of the negative imaginary part of the complex frequency of the mode, $\text{Im}(\omega_i^Q) = -0.04212 \text{ ps}^{-1}$. We have also observed the coupling of this mode with an outgoing wave packet on each side of the horizon, confirming the quasi-bound nature of this excited state. We have varied the frequency of the incoming wave packet and observed that the ringdown was not significantly affected. So the oscillation frequency $\text{Re}(\omega_i^Q)$ is the characteristic ringdown frequency of the horizon, and the observed localised mode is a quasinormal mode (QNM) of the horizon. Spatially, the bound part of the QNM is located near the horizon at $x = 0$ and the transverse width of the horizontal and vertical correlation features indicate that it extends over $10 \mu\text{m}$.

The oscillating pattern of the strictly horizontal and vertical features is due to a phase difference between the bound part of the QNM and the outgoing modes, while their diagonal inclination implies that the QNM does not have a purely standing wave shape but oscillates in time. Note that the anomalous modulation of the correlations in both the up- and downstream region stem from these fringe patterns, so the QNM effectively modulates correlated emission by the Hawking effect [62]. Because of the simultaneous spontaneous excitation of correlated waves and QNMs in the two regions, the latter modify the Hawking spectrum: the frequency distribution of

the Bogoliubov excitations emitted upstream will not smooth as in conserved quantum fluids [40], but will exhibit peaks at the frequencies $\text{Re}(\omega_i^Q)$ of the QNMs and with widths give by $\text{Im}(\omega_i^Q)$. As a result, the QNMs increase the Hawking emission, which is in turn dominated by Bogoliubov excitations of frequencies $\text{Re}(\omega_i^Q)$. This is similar to the phenomenology observed in *eg* [48], but the source here is different: the instability of the black hole results from a dissipative quench and not from two-boundary interactions.

Discussion We showed how engineering the density of a quantum fluid of polaritons can enhance the emission and propagation of paired Bogoliubov excitations in a transsonic flow. Our work sheds light on the interplay between optical bistability and parametric amplification in fluids of light. The bistable behaviour of a system can thus be exploited to study field theoretic effects like the Hawking effect in the laboratory.

Here we observed the generation and propagation of paired Bogoliubov excitations of the quantum fluid on either side of a sonic horizon when supporting the density of the fluid at various points in the bistable regime. Support of an inhomogeneous fluid density and velocity may be achieved by changing the wavenumber of the pump. In an experiment, this is easily implemented with high spatial resolution (limited by the diffraction limit) thanks to spatial light modulators [63]. We found that supporting the density of fluid at the turning point of the bistability loop (the sonic point) yields Hawking correlations of the order of 10^{-3} of the fluid fraction over more than $100\mu\text{m}$. These are a tenfold and a four- to tenfold enhancement, respectively, compared to previous results and render the observation of the HE realistic.

Furthermore, we observed quasi-normal modes of the horizon, which manifest themselves as a quasi-bound mode in the steady state. Differently from [45, 64], the physics we observe here in the steady-state takes place after the ringdown phase and the horizon instability is initially driven by vacuum fluctuations and not a classical perturbation. In other words, quantum fluctuation at the horizon not only yield pairs by the Hawking effect but also perturb the horizon under a dissipative quench. This phenomenology confirms the potential of polaritonic quantum fluids for analogue gravity: the tunability that was exploited to identify the optimal configuration to observe the HE also provides novel associated phenomena that emerge naturally. Typically, the present interplay with QNMs was, to our knowledge, never observed in similar configurations in conservative platforms such as atomic condensates, while it is relevant to black holes physics in general. Finally, our methods open the way to the theoretical and experimental study of the quantum statistics of the HE in driven-dissipative systems: for example, one could calculate (and observe) the Hawking correlations in reciprocal space [39], thus gaining frequency-resolved information on them [40] which could in turn be used to measure entanglement [30, 31].

ACKNOWLEDGEMENTS

We thank Théo Torres for insightful discussions on QNMs, Michiel Wouters for discussions on dispersion in bistable fluids, Tangui Aladjidi for help with code speed-ups as well as computer power, and Yuhao Liu for his work early in the project.

-
- [1] S. W. Hawking, *Nature* **248**, 30 (1974).
 - [2] C. Barceló, S. Liberati, and M. Visser, *Living Reviews in Relativity* **14**, 3 (2011).
 - [3] M. J. Jacquet, S. Weinfurter, and F. König, *Philosophical Transactions of the Royal Society A: Mathematical, Physical and Engineering Sciences* **378**, 20190239 (2020).
 - [4] W. G. Unruh, *Physical Review Letters* **46**, 1351 (1981).
 - [5] M. Visser, *Classical and Quantum Gravity* **15**, 1767 (1998).
 - [6] T. G. Philbin, C. Kuklewicz, S. Robertson, S. Hill, F. König, and U. Leonhardt, *Science* **319**, 1367 (2008).
 - [7] G. Rousseaux, C. Mathis, P. Maïssa, T. G. Philbin, and U. Leonhardt, *New Journal of Physics* **10**, 053015 (2008).
 - [8] O. Lahav, A. Itah, A. Blumkin, C. Gordon, S. Rinott, A. Zayats, and J. Steinhauer, *Physical Review Letters* **105**, 240401 (2010).
 - [9] S. Weinfurter, E. W. Tedford, M. C. J. Penrice, W. G. Unruh, and G. A. Lawrence, *Physical Review Letters* **106**, 021302 (2011).
 - [10] J.-C. Jaskula, G. B. Partridge, M. Bonneau, R. Lopes, J. Ruaudel, D. Boiron, and C. I. Westbrook, *Physical Review Letters* **109**, 220401 (2012).
 - [11] H. S. Nguyen, D. Gerace, I. Carusotto, D. Sanvitto, E. Galopin, A. Lemaître, I. Sagnes, J. Bloch, and A. Amo, *Physical Review Letters* **114**, 036402 (2015).
 - [12] L.-P. Euvé, S. Robertson, N. James, A. Fabbri, and G. Rousseaux, *Physical Review Letters* **124**, 141101 (2020).
 - [13] T. Torres, S. Patrick, A. Coutant, M. Richartz, E. W. Tedford, and S. Weinfurter, *Nature Physics* **13**, 833 (2017).
 - [14] S. Eckel, A. Kumar, T. Jacobson, I. Spielman, and G. Campbell, *Physical Review X* **8**, 021021 (2018).
 - [15] D. Vocke, C. Maitland, A. Prain, K. E. Wilson, F. Biancalana, E. M. Wright, F. Marino, and D. Faccio, *Optica* **5**, 1099 (2018).
 - [16] M. Wittemer, F. Hakelberg, P. Kiefer, J.-P. Schröder, C. Fey, R. Schützhold, U. Warring, and T. Schaetz, *Physical Review Letters* **123**, 180502 (2019).
 - [17] S. Patrick, H. Goodhew, C. Gooding, and S. Weinfurter, *Physical Review Letters* **126**, 041105 (2021).
 - [18] L.-P. Euvé, F. Michel, R. Parentani, T. G. Philbin, and G. Rousseaux, *Physical Review Letters* **117**, 121301 (2016).
 - [19] J. R. Muñoz de Nova, K. Golubkov, V. I. Kolobov, and J. Steinhauer, *Nature* **569**, 688 (2019).
 - [20] D. Campo and R. Parentani, *Physical Review D* **74**, 025001 (2006).
 - [21] S. Giovanazzi, *Physical Review Letters* **106**, 011302 (2011).
 - [22] X. Busch and R. Parentani, *Physical Review D* **89**, 105024 (2014).
 - [23] S. Finazzi and I. Carusotto, *Physical Review A* **90**, 033607 (2014).
 - [24] J. R. Muñoz de Nova, F. Sols, and I. Zapata, *Physical Review A* **89**, 043808 (2014).
 - [25] J. R. Muñoz de Nova, F. Sols, and I. Zapata, *New Journal of Physics* **17**, 10.1088/1367-2630/17/10/105003 (2015).

- [26] D. Boiron, A. Fabbri, P.-E. Larré, N. Pavloff, C. I. Westbrook, and P. Ziñ, *Physical Review Letters* **115**, 025301 (2015).
- [27] A. Finke, P. Jain, and S. Weinfurter, *New Journal of Physics* **18**, 113017 (2016).
- [28] A. Coutant and S. Weinfurter, *Physical Review D* **97**, 025005 (2018).
- [29] A. Coutant and S. Weinfurter, *Physical Review D* **97**, 025006 (2018).
- [30] M. Jacquet and F. König, *SciPost Physics Core* **3**, 005 (2020).
- [31] M. Isoard, N. Milazzo, N. Pavloff, and O. Giraud, *arXiv:2102.06175* (2021).
- [32] I. Carusotto, S. Fagnocchi, A. Recati, R. Balbinot, and A. Fabbri, *New Journal of Physics* **10**, 103001 (2008).
- [33] R. Balbinot, A. Fabbri, S. Fagnocchi, A. Recati, and I. Carusotto, *Physical Review A* **78**, 021603 (2008).
- [34] R. Parentani, *Physical Review D* **82**, 10.1103/PhysRevD.82.025008 (2010).
- [35] P.-E. Larré, A. Recati, I. Carusotto, and N. Pavloff, *Physical Review A* **85** (2012).
- [36] F. Michel, J.-F. Coupechoux, and R. Parentani, *Physical Review D* **94**, 084027 (2016).
- [37] Y.-H. Wang, M. Edwards, C. Clark, and T. Jacobson, *SciPost Physics* **3**, 022 (2017).
- [38] S. Robertson, F. Michel, and R. Parentani, *Physical Review D* **96**, 045012 (2017).
- [39] A. Fabbri and N. Pavloff, *SciPost Physics* **4**, 10.21468/SciPostPhys.4.4.019 (2018).
- [40] M. Isoard and N. Pavloff, *Physical Review Letters* **124**, 060401 (2020).
- [41] M. J. Jacquet, T. Boulier, F. Claude, A. Maître, E. Cancelleri, C. Adrados, A. Amo, S. Pigeon, Q. Glorieux, A. Bramati, and E. Giacobino, *Philosophical Transactions of the Royal Society A: Mathematical, Physical and Engineering Sciences* **378**, 20190225 (2020).
- [42] S. Chandrasekhar and S. Detweiler, *Proceedings of the Royal Society of London. A. Mathematical and Physical Sciences* **344**, 441 (1975), publisher: Royal Society.
- [43] E. Berti, V. Cardoso, and A. O. Starinets, *Classical and Quantum Gravity* **26**, 163001 (2009).
- [44] R. A. Konoplya and A. Zhidenko, *Reviews of Modern Physics* **83**, 793 (2011).
- [45] T. Torres, S. Patrick, M. Richartz, and S. Weinfurter, *Physical Review Letters* **125**, 011301 (2020).
- [46] C. Barceló, A. Cano, L. J. Garay, and G. Jannes, *Physical Review D* **74**, 024008 (2006).
- [47] S. Finazzi and R. Parentani, *New Journal of Physics* **12**, 095015 (2010).
- [48] I. Zapata, M. Albert, R. Parentani, and F. Sols, *New Journal of Physics* **13**, 10.1088/1367-2630/13/6/063048 (2011).
- [49] U. Leonhardt, T. Kiss, and P. Öhberg, *Physical Review A* **67**, 033602 (2003).
- [50] D. D. Solnyshkov, H. Flayac, and G. Malpuech, *Physical Review B* **84**, 233405 (2011).
- [51] P. Grišins, H. S. Nguyen, J. Bloch, A. Amo, and I. Carusotto, *Physical Review B* **94**, 144518 (2016).
- [52] D. Gerace and I. Carusotto, *Physical Review B* **86**, 144505 (2012).
- [53] A. Baas, J. P. Karr, H. Eleuch, and E. Giacobino, *Phys. Rev. A* **69**, 023809 (2004).
- [54] In the case where the pump's intensity is zero in the downstream region, the fluid coming from upstream will propagate ballistically there, as in eg [11, 51, 52]. The fluid density will decrease away from the horizon while the flow velocity will always be supersonic. In this case, the dispersion in the downstream region will be [65] $\omega_{\pm}^{\text{bal}} = \pm \sqrt{\frac{\hbar(k-k_0)^2}{2m} \left(\frac{\hbar(k-k_0)^2}{2m} + 2gn \right)} + v(k-k_0) - i\gamma/2$, where $k_0 = mv/\hbar$ denotes the wavevector of the ballistic fluid. It is the same sonic Bogoliubov dispersion relation as for $\Delta_p = gn$.
- [55] We remark that the 'speed of sound' is an ill-defined concept in such highly dispersive media as our quantum fluid of polaritons. However, it is generally accepted that the 'local speed of sound' c_s is given by the gradient of the tangent of the dispersion relation at $\omega = 0$ in the frame co-moving with the fluid. A sub-(super-)sonic flow is thus a flow for which v is lower (larger) than this gradient. In that sense, it is possible to define a horizon and to consider the region downstream from it as its inner region although there may be waves that propagate in both directions therein. There exist stricter definitions of the curvature of the effective spacetime in analogue gravity, see eg [30], but the related considerations do not impact the conclusions we draw in the present work.
- [56] M. Isoard, *Theoretical study of quantum correlations and non-linear fluctuations in quantum gases*, Ph.D. thesis, Université Paris-Saclay (2020).
- [57] J. Macher and R. Parentani, *Physical Review D* **79**, 124008 (2009).
- [58] A. Recati, N. Pavloff, and I. Carusotto, *Phys. Rev. A* **80**, 043603 (2009).
- [59] S. Hod, *Physics Letters B* **749**, 167 (2015).
- [60] S. R. Dolan and D. Dempsey, *Class. Quantum Grav.* **32**, 184001 (2015).
- [61] S. R. Dolan, *Physical Review D* **82**, 104003 (2010).
- [62] Remark that the difference in intensity of correlations between the up- and down-stream regions is due to the normalisation of the $g^{(2)}$ function. In fact the much lower fluid density downstream increases the intensity of the correlations in the North-West quadrant. Moreover, the fact that the density decreases spatially in this region gives the impression that the correlations do not decay in space, as the unnormalised correlations must do due to the finite lifetime γ of polaritons.
- [63] F. Claude, S. V. Koniakhin, S. V. Koniakhin, A. Maître, S. Pigeon, G. Lerario, D. D. Stupin, Q. Glorieux, Q. Glorieux, E. Giacobino, D. Solnyshkov, D. Solnyshkov, G. Malpuech, A. Bramati, and A. Bramati, *Optica* **7**, 1660 (2020).
- [64] S. Patrick, A. Coutant, M. Richartz, and S. Weinfurter, *arXiv:1801.08473 [gr-qc]* (2018).
- [65] I. Carusotto and C. Ciuti, *Review of Modern Physics* **85**, 299 (2013).
- [66] Unless specified otherwise, we write one-dimensional in reference to the spatial dimension of the system. There is always one temporal dimension in addition.
- [67] C. Ciuti and I. Carusotto, *physica status solidi (b)* **242**, 2224 (2005).
- [68] E. Wertz, L. Ferrier, D. D. Solnyshkov, R. Johne, D. Sanvitto, A. Lemaître, I. Sagnes, R. Grousson, A. V. Kavokin, P. Senellart, G. Malpuech, and J. Bloch, *Nature Physics* **6**, 860 (2010).
- [69] S. Pigeon and A. Aftalion, *Physica D: Nonlinear Phenomena* **415**, 132747 (2021).
- [70] R. Brout, S. Massar, R. Parentani, and P. Spindel, *Physical Review D* **52**, 4559 (1995).
- [71] S. Corley and T. Jacobson, *Physical Review D* **54**, 1568 (1996).
- [72] M. Wouters and I. Carusotto, *Physical Review A* **76**, 043807 (2007), publisher: American Physical Society.
- [73] The existence of *in* GMs in the downstream region is a specificity of the superluminal dispersion relation of polariton and atomic quantum fluids.

- [74] M. J. Jacquet and F. König, Physical Review A **102**, 013725 (2020).
 [75] I. Carusotto and C. Ciuti, Phys. Rev. B **72**, 125335 (2005).
 [76] S. Pigeon and A. Bramati, New Journal of Physics **19**, 095004 (2017).

APPENDIX

Appendix A: The physical system

Our system is a one-dimensional[66] quantum fluid of exciton-polaritons whose flow velocity goes from being sub- to super-sonic, thus forming a sonic horizon where the local flow velocity of the fluid equals the local speed of sound. For simplicity, we may consider that the horizon separates two spatial regions whose properties are independent of space — two homogenous regions, although we shall eventually depart from this simplified picture. For now, we begin with the theoretical description of a homogeneous quantum fluid (of its phase and density) and of the propagation of quantum (i.e. small-amplitude density) fluctuations therein.

1. Polariton fluid and Bogoliubov excitations

Exciton-polaritons are quasi-particles resulting from the interaction of light with matter in a semiconductor microcavity. Photons emitted by a laser will be trapped in a cavity formed by two Bragg mirror, wherein their dispersion is the usual Fabry-Perot dispersion. These trapped photons create excitons — bound electron-hole pairs — in the semiconductor microcavity. Strong coupling between the photons and excitons trapped in quantum wells gives rise to two eigenstates for the total Hamiltonian, known as the lower polariton (LP) and upper polariton (UP) branches. Furthermore, the Coulomb interaction between excitons results in an effective non-linearity for exciton-polaritons (polaritons). The dynamics of the mean-field are governed by a generalised Gross-Pitaevskii equation, which leads to Euler and continuity equations describing the system as a quantum fluid. Historically, polaritons have first been described as two-dimensional quasi-particles [67], although the theory may be reduced to one-dimensional cavities called ‘wires’ [11, 51, 52, 68], as in the present case.

In the majority of cases, all energies involved are small compared to the Rabi splitting so the exciton-polariton system can be described by the mean field approximation [65]. At this level the system is described by a single scalar field Ψ , the field of lower polaritons, whose dynamics are governed by the driven-dissipative Gross-Pitaevskii equation (GPE)

$$i\partial_t \Psi(x, t) = \left[\omega_0 - \frac{\hbar}{2m} \partial_x^2 + V(x) + g|\Psi(x, t)|^2 - i\frac{\gamma}{2} \right] \Psi + F_p(x, t). \quad (\text{A1})$$

ω_0 is the frequency of the lower polaritons at the bottom of the branch, m is their effective mass, V is the ‘external potential’

(that is controlled via the interplay of the density profile of the pump and the cavity’s own potential), g is the effective non-linearity, γ is the loss rate, F_p is the field of the pump laser. The field $\Psi(x, t)$ is written in the laboratory frame.

The description of the system as a fluid is supported by the Madelung transformation: we write the field of lower polaritons as $\Psi(x, t) = \sqrt{n(x, t)}e^{i\theta(x, t)}$, insert this expression into (A1) and multiply by $e^{-i\theta}\sqrt{n}$, thus obtaining

$$\begin{aligned} e^{-i\theta}i\partial_t(\sqrt{n}e^{i\theta}) &= \frac{1}{2}i\partial_t n - n\partial_t\theta, \\ e^{-i\theta}\partial_x^2(\sqrt{n}e^{i\theta}) &= n(\partial_x\theta)^2 + \sqrt{n}\partial_x^2\sqrt{n} + i\partial_x(n\partial_x\theta). \end{aligned} \quad (\text{A2})$$

We write $v = \frac{\hbar}{m}\partial_x\theta$ and insert (A2) into (A1), so that, by taking the real and imaginary parts, we arrive at the Euler and continuity equations for the polariton fluid [69]:

$$\begin{aligned} \partial_t\theta + \frac{mv^2}{\hbar} + \frac{\hbar}{2m}\frac{\partial_x^2\sqrt{n}}{\sqrt{n}} + V + gn + \frac{\text{Re}\{F_p e^{-i\theta}\}}{\sqrt{n}} &= 0, \\ \partial_t n + \partial_x(nv) &= \gamma n - 2\text{Im}\{F_p e^{-i\theta}\}\sqrt{n}. \end{aligned} \quad (\text{A3})$$

The first equation of (A3) is the Euler equation of atomic Bose-Einstein condensates (BECs) plus a term coming from the coherent pumping. The second equation of (A3) is the continuity of the flow with a loss term and a term coming from the coherent pumping. We see that the properties of the fluid depend on two parameters, namely its’ density n and phase θ . The spatial variations of the phase is encapsulated in v , which we identify from (A3) as the flow velocity of the fluid.

Now that we have described the polariton fluid in terms of its’ density and phase, we consider the propagation of small amplitude fluctuations (such as quantum fluctuations) of the density in this fluid — the so-called ‘Bogoliubov excitations’. Bogoliubov excitations are mathematically obtained by linearising the GPE (A1) around a background: $\Psi \rightarrow \Psi + \delta\Psi$, and $\Psi^* \rightarrow \Psi^* + \delta\Psi^*$. \mathcal{L} is the ‘Bogoliubov matrix’ that describes the dynamics of the Bogoliubov excitations $(\delta\Psi, \delta\Psi^*)$: $i\partial_t \begin{pmatrix} \delta\Psi \\ \delta\Psi^* \end{pmatrix} = \mathcal{L} \begin{pmatrix} \delta\Psi \\ \delta\Psi^* \end{pmatrix}$.

In the steady state, the GPE (A1) becomes

$$\left[\omega_0 - \omega_p - \frac{\hbar}{2m} \partial_x^2 + V(x) + g|\Psi(x)|^2 - i\frac{\gamma}{2} \right] \Psi(x) + F_p(x) = 0, \quad (\text{A4})$$

where ω_p is the frequency of the pump. We first consider a configuration where the wire is pumped with a spatially homogeneous and monochromatic pump of incident wavevector k_p (so there is no potential in Eq. (A1), $V(x) = 0$). The phase of the fluid is then set by, and equal to, k_p while its’ density is homogeneous. The steady-state GPE (A4) simplifies to

$$\left[g|\Psi|^2 - \Delta_p - i\frac{\gamma}{2} \right] \Psi + F_p = 0, \quad (\text{A5})$$

where Δ_p is the ‘effective detuning’ defined as the difference between the pump energy and that of lower polaritons,

$$\Delta_p = \omega_p - \omega_0 - \frac{\hbar k_p^2}{2m}. \quad (\text{A6})$$

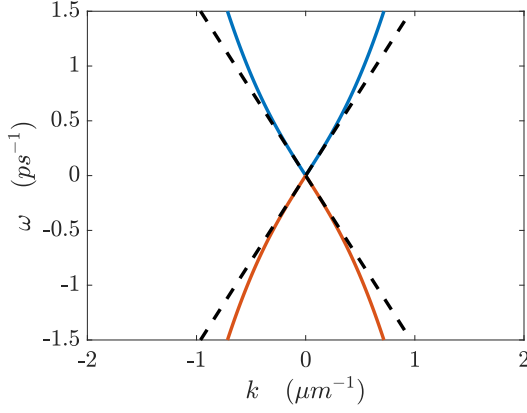


Figure 4. **Dispersion curve of the polaritonic fluid in the frame co-moving with the fluid.** Real part of the dispersion (A8) for a pump vector $k_p = 0.25 \mu\text{m}^{-1}$. Blue, $\omega_+^{\Delta p=gn}$; orange, $\omega_-^{\Delta p=gn}$. Black dashed lines show the speed of sound.

We go to the reference frame co-moving with the fluid via a Galilean transform ($x \rightarrow x - vt$). In the special case of a homogeneous system where the interaction energy matches the detuning, $gn = \Delta_p$, the Bogoliubov matrix \mathcal{L} can be written in this frame as

$$\mathcal{L} = \begin{pmatrix} gn + \frac{\hbar k^2}{2m} + i\gamma/2 & gne^{2ik_p x} \\ gne^{-2ik_p x} & gn + \frac{\hbar k^2}{2m} - i\gamma/2 \end{pmatrix}. \quad (\text{A7})$$

Upon diagonalization, we retrieve the Bogoliubov dispersion relation in this co-moving frame, which relates the wavenumber k of Bogoliubov excitations to their frequency ω there:

$$\omega_{\pm}^{\Delta p=gn} = \pm \sqrt{\frac{\hbar k^2}{2m} \left(\frac{\hbar k^2}{2m} + 2gn \right)} - i\gamma/2. \quad (\text{A8})$$

Figure 4 shows the real part of Eq. (A8), the ‘dispersion curve’, which is identical to that of atomic BECs. There are two branches $\omega_{\pm}^{\Delta p=gn}$ of the dispersion, which are symmetrical around the point $\omega = 0, k = 0$. At low k , the dispersion curve has a linear slope: $\omega_{\pm}^{\Delta p=gn} \xrightarrow[k \rightarrow 0]{} c_s k$, with $c_s = \sqrt{\hbar gn/m}$ the ‘speed of sound’ in the fluid. At large k , the dispersion is that of free massive particles, $\omega_{\pm}^{\Delta p=gn} \xrightarrow[k \rightarrow \infty]{} \hbar k^2/2m$. There, $\left| \partial \omega_{\pm}^{\Delta p=gn} / \partial k \right| > c_s$ — the gradient of the dispersion curve is larger than the speed of sound, so the dispersion is said to be ‘superluminal’ (in analogy with superluminal corrections to the dispersion in eg [70, 71]).

2. Optical bistability of the polariton fluid

Unlike the configuration considered in the previous paragraph, in the majority of cases the interaction energy does not match the effective detuning and the dispersion curve is thus modified. Furthermore, writing the density of the fluid as a function of the intensity of the laser yields several solutions. This degeneracy of fluid densities is due to optical bistability, which, as we will show, has tremendous influence on the

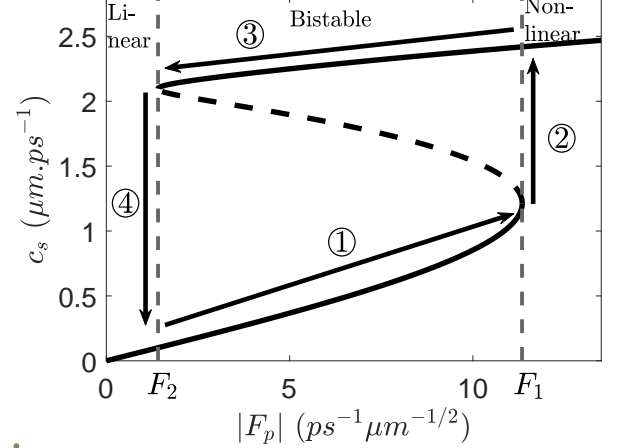


Figure 5. **Bistability loop for an homogeneous polaritonic fluid.** $\omega_p - \omega_0 > 0$ and $k_p = 0$. Black, stable points; dashed, unstable points. The system is bistable for $F_2 < |F_p| < F_1$ and follows the hysteresis cycle (1)-(4).

emission and propagation of excitations of the fluid, including Bogoliubov excitations. Here we investigate the influence of the bistability on the Bogoliubov dispersion.

We begin by describing the relationship between the density of polaritons, n , and the intensity of the pump laser, $|F_p|^2$ in the case where the energy of the laser is above that of the lower polaritons, $\Delta_p > \gamma\sqrt{3}/2$: we square Eq. (A5) and find

$$\begin{aligned} \left[(gn - \Delta_p)^2 + \frac{\gamma^2}{4} \right] n &= |F_p|^2 \\ \left[\left(\frac{mc_s^2}{\hbar} - \Delta_p \right)^2 + \frac{\gamma^2}{4} \right] \frac{mc_s^2}{g\hbar} &= |F_p|^2. \end{aligned} \quad (\text{A9})$$

The physics at play may be investigated equivalently in terms of the relationship between the speed of sound and the strength of the pump, as shown in Figure 5. At first, c_s increases slowly with $|F_p|$ (arrow (1)), until $|F_p| = F_1$ where it increases abruptly (arrow (2)). For $|F_p| > F_1$, c_s increases slowly again. If the pump’s strength is decreased from $|F_p| \geq F_1$, c_s decreases slowly until $|F_p| = F_2$ (arrow (3)), where it falls abruptly (arrow (4)). Since $F_1 > F_2$, the c_s to $|F_p|$ relationship presents a hysteresis cycle with two regimes of speed of sound: the linear regime when $|F_p| < F_1$ and c_s is low, and the non-linear regime when $|F_p| > F_2$ and c_s is high. This hysteresis cycle is the manifestation of optical bistability [53], so we will henceforth refer to it as the ‘bistability loop’. Note that the dashed line in Fig. 5 is unstable and the speed of sound will actually follow the hysteresis cycle schematised by arrows (1) – (4).

Now, in order to explicitly show the dependence of the Bogoliubov dispersion on the density of the fluid as well as the influence of optical bistability thereon, we generalise Eq. (A8): We diagonalise the Bogoliubov matrix \mathcal{L} for a ho-

homogeneous system pumped with arbitrary strength and obtain

$$\omega_{\pm}(k) = \pm \sqrt{\left(\frac{\hbar k^2}{2m} + 2gn - \Delta_p\right)^2 - (gn)^2 - i\gamma/2}. \quad (\text{A10})$$

In Fig. 6, we show the dispersion curve for 5 different fluid densities along the bistability loop. As can be seen in Fig. 6 **a)** and **b)**, the shape of the dispersion does not change much in the linear regime: the two branches of the dispersion curve cross. When the fluid is bistable, in Fig. 6 **b)**, we observe the appearance plateaus characteristic of an unstable fluid at the crossing points — Goldstone modes [72]. On the other hand, the shape of the dispersion curve changes significantly in the nonlinear regime depending on the position along the bistability loop: at high pump strength (Fig. 6 **e)**), the two branches are split in energy by a gap that increases with the pump strength. The sonic dispersion relation (A8) is recovered at point *C* (Fig. 6 **c)**), while for slightly lower pump strength (Fig. 6 **d)**), the plateau at low *k* is characteristic of an unstable fluid (similarly to the Goldstone modes of Fig. 6 **d)**). Note that the dispersion curve has a linear slope at low *k* (and thus a sonic interpretation) at point *C* only, which is thus sometimes referred to as the ‘sonic point’ of the bistability. As Eq. (A10) is of order four in *k*, the dispersion has four complex roots. The real part of these roots is non-zero in the linear regime (Fig. 6 **a)** and **b)**) as well as at points *C* and *C'* (Fig. 6 **c)** and **d)**), but not at point *D* (Fig. 6 **e)**).

In this appendix, we have seen that the mean-field of a polariton system behaves as a fluid. We have studied the dispersion relation of Bogoliubov excitations in this fluid and seen that optical bistability of the fluid strongly influences the properties of this dispersion relation. These considerations may be generalised to a fluid whose density is not homogeneous.

3. Dispersion relation in the nonlinear regime

In Fig. 7, we plot the dispersion relation (2) of the inhomogeneous fluid in the laboratory frame when pumping at point *D* of the bistability loop (see Fig. 6 **e)**): Fig. 1 **a)** and **b)** show the dispersion of a sub- and super-sonic fluid flow, respectively. Blue (orange) curves correspond to positive (negative) energy solutions of Eq. (A10) in the frame co-moving with the fluid. As usual in field theories in analogue gravity, the modes with positive (negative) energies in the rest frame of the fluid have positive (negative) Klein-Gordon norm [56]. For subsonic fluid flows, the negative norm branch is at negative laboratory frame energies, while for supersonic flows, part of the negative norm branch is pulled up to positive laboratory frame energies by the Doppler effect, up to a maximum energy which we denote by ω_{max} . Note that the dispersion up- and downstream features a gap between the positive- and negative-norm branches. We denote the minimum energy of the positive-norm branch in the upstream region by ω_{min} .

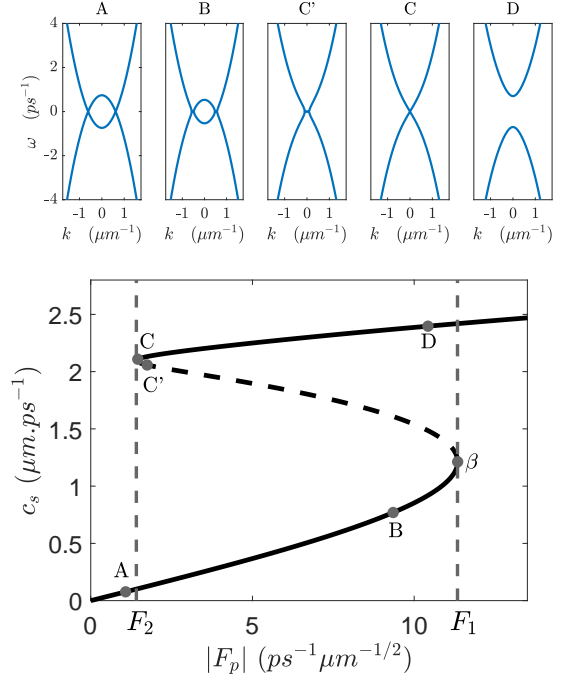


Figure 6. **Bogoliubov dispersion for various fluid densities.** Top row: Eq.(A10) is plotted in the fluid frame. **a)** and **b)**, linear regime of density; **c)**, Goldstone modes; **d)**, sonic dispersion; **e)** nonlinear regime of density. Bottom, **f)**, bistability curve for a homogeneous fluid. **A**, linear; **B**, linear and bistable; **C'**, unstable; **C**, sonic point; **D** nonlinear and bistable.

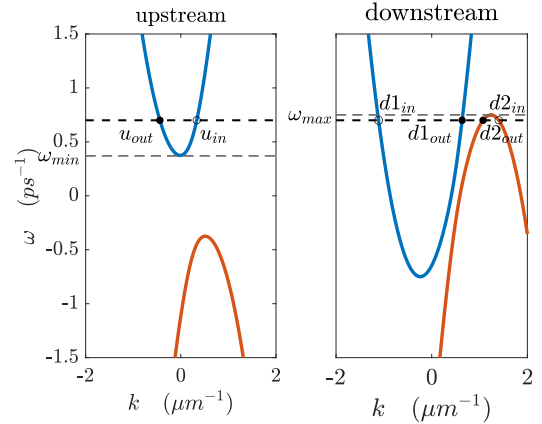


Figure 7. **Laboratory frame dispersion relation in the nonlinear regime.** Left (right) column, dispersion relation (2) for a sub-sonic (supersonic) fluid flow. Blue, positive-norm branch; orange, negative-norm branch. Circles, local modes of positive group velocity; filled dots, local modes of negative group velocity. Dot-dashed line, ω_{max} ; dotted line, ω_{min} ; dashed line ω_0 . Pump strength and speed of sound at point *D* in Fig. 6.

4. Global Modes of the system

In this appendix we explain how to construct the global modes (GMs) of the system from the local modes (LMs) identified in the body of the article.

LMs in a homogeneous region may be sorted by their

respective group velocity $v_g = \partial\omega_{\pm}/\partial k$: those which have positive group velocity propagate rightwards while those which have negative group velocity propagate leftwards. We proceed to construct modes of the inhomogeneous fluid, the GMs [56, 57] — solutions to the equation of motion that are valid in both regions on either sides of the interface. GMs correspond to waves scattering at the interface, and they describe the conversion of an incoming field to scattered fields in both regions. The GMs are superpositions of the plane wave solutions in the two homogeneous regions on either side of the interface. We identify GMs via their ‘defining’ local mode. Specifically, in the upstream region, the unique local mode with positive group velocity defines an *in* GM u_{in} , while the unique local mode with negative group velocity defines an *out* GM u_{out} . In the downstream region, modes with negative group velocity define *in* GMs d_{1in} and d_{2out} and modes with positive group velocity define *out* GMs d_{1out} and d_{2out} [73]. GMs u_{in} , u_{out} , d_{1in} and d_{1out} are positive-norm modes while GMs d_{2in} and d_{2out} are negative-norm modes.

Each *in* GM describes the scattering of a harmonic wave to various outgoing harmonic waves. Conversely, each *out* GM describes a single harmonic wave resulting from the scattering of various incoming waves. The scattering can be described in the *in* as well as the *out* basis, and the transformation between the two bases defines the scattering matrix (see [35, 56, 57, 74] for an analytical derivation of the scattering matrix). Because the vacuum is basis dependent, spontaneous emission at the horizon will occur in correlated pairs $u_{out}-d_{1out}$, $u_{out}-d_{2out}$ and $d_{1out}-d_{2out}$ on top of the classical background formed by the polariton fluid (the mean-field).

Appendix B: Numerical method and correlation function

Our interest is in spontaneous emission, that is amplification of the quantum vacuum fluctuations at the horizon (the *spontaneous* Hawking effect). The quantum description of the Bogoliubov excitations relies on the dispersion relation of the classical field, Eq. (2). In order to encompass quantum effects, we use a quantum Monte-Carlo method called the truncated Wigner approximation (TWA). In this method, the Wigner distribution is truncated so as to map it to a stochastic partial differential equation for a classical field ψ :

$$i d\psi = \left[\omega_0 - \frac{\hbar}{2m} \frac{d^2}{dx^2} + V + g(|\psi|^2 - 1/\Delta x) - i\frac{\gamma}{2} \right] \psi dt + F_p dt + \sqrt{\frac{\gamma}{4\Delta x}} dW, \quad (B1)$$

where dW is complex white noise. In numerical simulations, sampling of the realisations obtained with (B1) starts when the steady state is reached. One must ensure that enough time is spent between each sampling to ensure independence of the realisations. Quantum observables are computed with statistical averaging over the realisations obtained with the TWA:

the general rule for N arbitrary observables is [75]

$$\langle O_1 \dots O_N \rangle_W = \frac{1}{N!} \sum_{\text{All } N\text{-permutations}} \langle P(\hat{O}_1, \dots, \hat{O}_N) \rangle, \quad (B2)$$

where $\langle \rangle_W$ denotes the statistical averaging over the realisations. Note that the TWA is valid at the level of the Bogoliubov theory only.

Emission at the horizon by the Hawking effect is best detected via nonlocal correlations in the fluid density [32]. These may be quantified via the normalised spatial correlation function

$$g^{(2)}(x, x') = \frac{G^{(2)}(x, x')}{G^{(1)}(x)G^{(1)}(x')}. \quad (B3)$$

$G^{(2)}(x, x')$ is the diagonal four-points correlation function of the field, which is calculated from (B2) and normally ordered using Bose statistics:

$$\begin{aligned} G^{(2)}(x, x') &= \langle \hat{\Psi}^\dagger(x) \hat{\Psi}^\dagger(x') \hat{\Psi}(x') \hat{\Psi}(x) \rangle \\ &= \langle \psi^*(x) \psi^*(x') \psi(x') \psi(x) \rangle_W - \frac{1}{\Delta x} (1 + \delta_{x, x'}) \times \\ &\quad \left(\langle \psi^*(x) \psi(x) \rangle_W + \langle \psi^*(x') \psi(x') \rangle_W - \frac{1}{2\Delta x} \right), \end{aligned} \quad (B4)$$

while the diagonal two-points correlation function is

$$G^{(1)}(x) = \langle \hat{\Psi}^\dagger(x) \hat{\Psi}(x) \rangle = \langle \psi^*(x) \psi(x) \rangle_W - \frac{1}{2\Delta x}. \quad (B5)$$

In this Appendix we have shown how microcavity polaritons behave as a quantum fluid whose velocity is determined by its phase, and in which the speed of sound is proportional to the fluid density. We have studied the kinematics of Bogoliubov excitations in this fluid and identified the conditions under which a transsonic fluid flow features a sonic horizon. Correlated emission at the horizon by the Hawking effect may be characterised by the correlation function, which is calculated from the output of numerical simulations with the TWA.

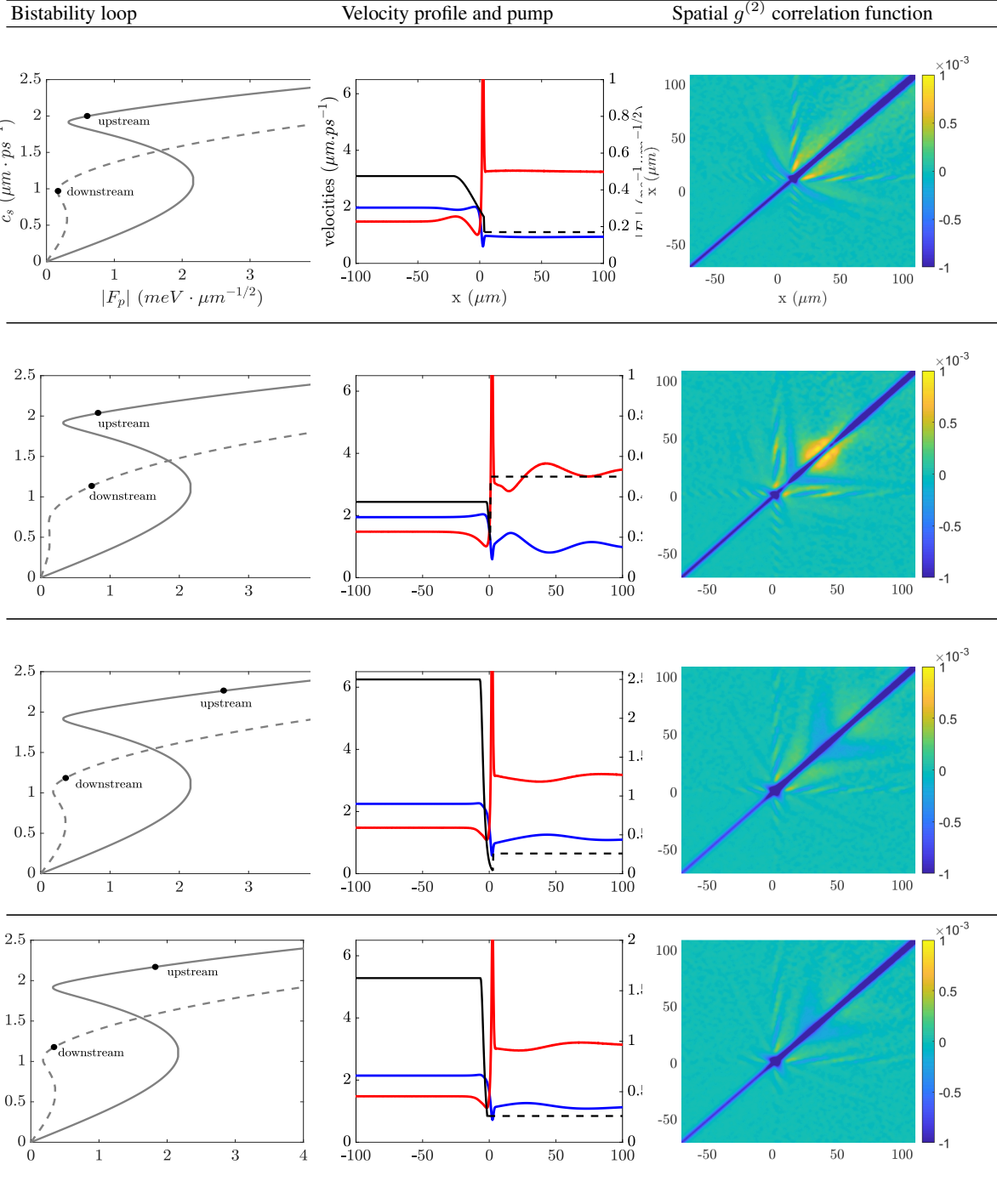
Appendix C: Influence of Optical bistability on emission by the Hawking effect

In this Appendix we calculate spatial correlation spectra across the horizon for various flow profiles (density and phase) on either side of the horizon. Importantly, the detuning $\omega_p - \omega_0 = 0.49$ meV is kept constant throughout for comparison between simulations. Alternatively, the optical bistability of the system could be tuned by varying the detuning while keeping some other parameters constant. All spectra result from 100 000 Monte-Carlo realisations.

As we have seen in Appendix A 2, it is possible to tune the bistability of the fluid on either side of the horizon by controlling the wavevector (i.e. the phase) of the fluid in either region by means of the pump ($k_{p,u}$ or $k_{p,d}$ in the up- or downstream

region, respectively), while the fluid density may be supported on the higher branch of the hysteresis loop by means of the Pigeon effect [76]. There are, roughly speaking, 6 different points along the bistability loop (see Fig. 5), meaning that in order to explore the full parameter space we have computed

36 correlation spectra. Not all combinations are interesting, though, so here we will only comment on spatial correlations obtained with typical (and relevant) inhomogeneous flow profiles.



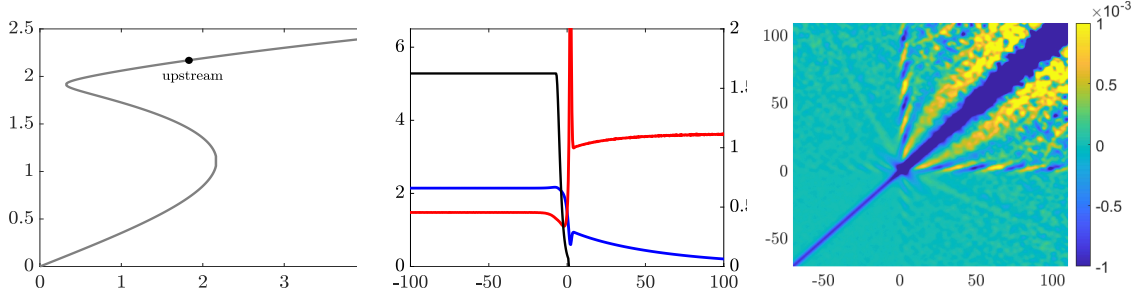


Table I: **Spectra of correlated emission at the horizon.** **Left column**, bistability loop: solid black, upstream region; dashed gray, downstream region. **Middle column**, solid black, pump strength upstream ($k_{p,u}$); dashed black, pump strength downstream ($k_{p,d}$); blue, speed of sound; red, fluid flow velocity $k_{p,u}$. **Right column**, spatial $g^{(2)}$ correlation function (B3), colour scale from -10^{-3} to 10^{-3} .

In Table I we plot the operation point on the bistability loop of the fluid on either side of the horizon, the pump profile and ensuing properties of the inhomogeneous fluid as well as the resulting spatial correlations (B3). Here we describe in detail each inhomogeneous fluid profile and the resulting correlations.

- I-1: The fluid density is supported near the sonic point in both regions, such that it is quite flat, with a phase fixed by $k_{p,u} = 0.25 \mu\text{m}^{-1}$ and $k_{p,d} = 0.545 \mu\text{m}^{-1}$, respectively. Anti-correlations along the diagonal are of large amplitude. The diagonal is broader in the downstream region than in the upstream region. The Hawking moustache $u_{out} - d2_{out}$ is of amplitude $6 \cdot 10^{-4}$ and is about $40 \mu\text{m}$ - and $50 \mu\text{m}$ -long in the up- and down regions, respectively. The $u_{out} - d1_{out}$ correlations are of amplitude $5 \cdot 10^{-4}$ and the trace is $25 \mu\text{m}$ and $60 \mu\text{m}$ long in the up- and downstream regions, respectively. The $d1_{out} - d2_{out}$ correlations are of amplitude $8 \cdot 10^{-4}$ and the trace is $50 \mu\text{m}$ long. Furthermore, local, positive correlations along the diagonal can be observed in both the up- and downstream regions.
- I-2: The fluid density is supported in the bistable regime in the upstream region while it is supported in the non-linear regime in the downstream region, with a phase fixed by $k_{p,u} = 0.25 \mu\text{m}^{-1}$ and $k_{p,d} = 0.58 \mu\text{m}^{-1}$, respectively. The density of the fluid undulates in the region $100 \mu\text{m}^{-1}$ after the horizon and stabilises afterwards. The Hawking moustache is of amplitude $2 \cdot 10^{-4}$ and is about $10 \mu\text{m}$ - and $20 \mu\text{m}$ -long in the up- and downstream regions, respectively. The $u_{out} - d1_{out}$ correlations are of amplitude $2 \cdot 10^{-4}$ and the trace is $20 \mu\text{m}$ and $20 \mu\text{m}$ long in the up- and downstream regions, respectively. After $20 \mu\text{m}$, both up-downstream correlation traces become dispersive. The $d1_{out} - d2_{out}$ correlation trace is not visible. Instead, it is masked by a new, emergent feature in the downstream region — an anti-correlation trace that begins at $20 \mu\text{m}$, which is followed by a positive, local-correlations trace that starts

at $50 \mu\text{m}$.

- I-3: The fluid density is in the highly-nonlinear regime in the upstream region, while it is supported on the upper branch of the bistable regime in the downstream region, with a phase fixed by $k_{p,u} = 0.25 \mu\text{m}^{-1}$ and $k_{p,d} = 0.535 \mu\text{m}^{-1}$, respectively. The Hawking moustache is of amplitude $2 \cdot 10^{-4}$ and is about $12 \mu\text{m}$ - and $17 \mu\text{m}$ -long in the up- and downstream regions, respectively. The $u_{out} - d1_{out}$ correlations are of amplitude $9 \cdot 10^{-5}$ and the trace is $10 \mu\text{m}$ and $25 \mu\text{m}$ long in the up- and downstream regions, respectively. The $d1_{out} - d2_{out}$ correlations are of amplitude $2 \cdot 10^{-4}$ and the trace is $50 \mu\text{m}$ long. Furthermore, negative correlations appear $30 \mu\text{m}$ downstream of the horizon, followed by positive correlations after $55 \mu\text{m}$.
- I-4: The fluid density is supported on the upper branch in the bistable regime in both regions, with a phase fixed by $k_{p,u} = 0.25 \mu\text{m}^{-1}$ and $k_{p,d} = 0.535 \mu\text{m}^{-1}$, respectively. The fluid density is homogeneous in the upstream region but not in the downstream region where it undulates. Note that, for reasons explained in appendix F, the strength of the defect potential is 30% lower than in all other configurations, yielding weaker spontaneous emission. The Hawking moustache is of amplitude $1 \cdot 10^{-4}$ and is about $12 \mu\text{m}$ - and $17 \mu\text{m}$ -long in the up- and downstream regions, respectively. The $u_{out} - d1_{out}$ correlations are of amplitude $8 \cdot 10^{-5}$ and the trace is $30 \mu\text{m}$ and $60 \mu\text{m}$ long in the up- and downstream regions, respectively. The $d1_{out} - d2_{out}$ correlations are of amplitude $3.5 \cdot 10^{-4}$ and the trace is $50 \mu\text{m}$ long. Furthermore, negative correlations appear $22 \mu\text{m}$ downstream of the horizon, followed by positive correlations after $50 \mu\text{m}$.
- I-5: The fluid density is supported on the upper branch in the bistable regime in the upstream region ($k_{p,u} = 0.25 \mu\text{m}^{-1}$), while it is left to evolve ballistically in the downstream region. The Hawking moustache is of am-

plitude $2 \cdot 10^{-4}$ and is about $20 \mu\text{m}$ - and $20 \mu\text{m}$ -long in the up- and downstream regions, respectively. The $u_{out} - d1_{out}$ correlations are of amplitude $1.3 \cdot 10^{-4}$ and the trace is $27 \mu\text{m}$ and $60 \mu\text{m}$ long in the up- and downstream regions, respectively. The $d1_{out} - d2_{out}$ correlations are of amplitude $3 \cdot 10^{-4}$ and the is $120 \mu\text{m}$ long.

In configuration I-1, 2, 3 and 4, we see that emission occurs even when the phase of the fluid is fixed by the pump in order to support its density on both sides of the horizon. However, correlation traces in the North West quadrant are short in these configurations, meaning that the propagation of Bogoliubov excitations in the downstream region is limited when the phase is fixed there. Furthermore, in configurations for which the fluid density undulates in the downstream region (I-3 and 4), other short positive- and negative-correlation traces appear well after the horizon. These correspond to spontaneous emission from the vacuum on an effective spacetime without a horizon but whose properties are not homogeneous [30].

Spontaneous emission also occurs when the density of the fluid evolves ballistically in the downstream region, as in configurations I-5 and in Fig.2, and as in [11, 51, 52]. In all these configurations, the downstream-downstream correlations $d1_{out} - d2_{out}$ as well as the the Hawking moustache are clearly visible. However, in [11, 51], the $u_{out} - d1_{out}$ correlations are not visible (if at all present), while they are in [52] and in Table. I-5 and in Fig.2. In [51], it was established that an effective cavity forms between the edge of the (Gaussian) pump and the defect. The Bogoliubov excitations in the upstream region form a standing wave in this effective cavity, which in turn modulates the emission of negative norm waves in the downstream region and thus that of the positive norm companion wave as well. The resulting modulation of the correlation pattern in the downstream region (North East quadrant) was observed in both [11] and [51]. This modulation might be why the up-downstream $u_{out} - d1_{out}$ are not visible in these works.

So far we have established that operating with a density at the sonic point of the bistability loop upstream of the horizon enhances the propagation of Bogoliubov excitations in the upstream region. In configuration I-1, we also consider the case where the fluid density is also supported at the sonic point in the downstream region. As observed before, the downstream-downstream trace corresponding to $d1_{out} - d2_{out}$ correlations is only of amplitude $8 \cdot 10^{-4}$, which is overpowered by a positive-correlation trace along the diagonal that stems from local interactions (unlike the physics under study). Yet, the up-downstream correlations are clearly visible and the two traces are over $60 \mu\text{m}$ long, which confirms that spontaneous emission by the Hawking effect does occur. In comparison, the Hawking moustache and all other correlation traces are stronger and longer in Fig.2. So letting the fluid density evolve ballistically in the downstream region enhances the emission and propagation of Bogoliubov excitations there.

Appendix D: Influence of the fluid properties near the horizon on spontaneous emission

In the body of the paper, we have evidence the crucial role of the control of the fluid density in the vicinity of the horizon in the propagation of Bogoliubov excitations. This is confirmed in the analysis of Appendix C. In this Appendix, we investigate the influence of the fluid density in the vicinity of the horizon on the emission of Bogoliubov excitations. Specifically, we compute the density of Bogoliubov excitations in the upstream region as a function of the fluid density before the horizon.

As Fig.2, we create the fluid of polaritons by pumping in the nonlinear regime far from the horizon in the upstream region. The fluid density is then supported at the sonic point until a given distance from the horizon, where the pump strength drops to zero abruptly. Thereafter, the fluid propagates ballistically to the horizon and across it into the downstream region. The fluid density is supported in the upstream region such that it dips slightly where the pump strength drops, and then bumps back up to the sonic point. In Fig. D, we compute the density of Bogoliubov excitations on top of the fluid,

$$\langle \delta \hat{\Psi}^\dagger(x) \delta \hat{\Psi}(x) \rangle = \langle \hat{\Psi}^\dagger(x) \hat{\Psi}(x) \rangle - |\Psi(x)|^2, \quad (\text{D1})$$

for different distances between the pump and the horizon. We see that the density of Bogoliubov excitations increases until a distance of $10 \mu\text{m}$. For short distances, the density is low because the accumulation of the fluid between the pump and the horizon forms a high bump where the density is above the sonic point. For distances larger than $10 \mu\text{m}$, the fluid density drops from the upper branch of the bistability loop and no emission occurs. The width of the peak in the spectrum of Bogoliubov excitations is different from the distance between the pump and the horizon. Note the difference between the density of Bogoliubov excitations in the up- and downstream regions: the difference decreases from six-fold for a $10 \mu\text{m}$ pump-horizon distance to less than three-fold for a $7 \mu\text{m}$ distance. This is mainly due to a decrease in the emission strength in the upstream region.

In Fig. D, we compute Eq.(D1) and vary the fluid density on top of the bump in the vicinity of the sonic point while keeping the distance between the drop in the pump strength of the horizon constant. We see that the density of Bogoliubov excitations in the upstream region drops quickly as the fluid density moves away from the sonic point. This indicates that the Hawking effect is less and less efficient. As we have seen before in Sec.A 2, the shape of the dispersion relation is highly influenced by the fluid density along the bistability loop. Here, we see that the dispersion curve quickly morphs from Fig. 6 d) to Fig. 6 e) and, as a result, the condition of momentum conservation at the heart of the Hawking effect, the mixing of modes of positive and negative norms at the horizon, is less and less fulfilled.

In brief: Bogoliubov excitations are emitted in the upstream region as long as the fluid density is supported on the upper branch of the bistability loop in the vicinity of the horizon. In this appendix, we have demonstrated that operating at exactly

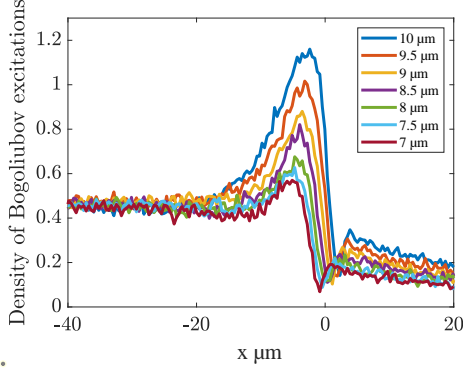


Figure 8. **Density of Bogoliubov excitations (D1) in the vicinity of the defect for various pump-horizon distance.** $k_{p,u} = 0.24 \mu\text{m}^{-1}$.

the sonic point there strongly enhances spontaneous emission and, in turn, propagation in the upstream region.

Appendix E: Fringes in the North-East, North-West and South-East quadrants

As described in section C, there are fringes along strictly horizontal and vertical directions in the correlation spectra in all configurations. These are visible in the South-East and North-West (*upstream-downstream*) and North-East (*downstream-downstream*) quadrants. Their anomalous correlation is thus non-zero, which creates an interference pattern in the $g^{(2)}$ function [51]. As for the *up-downstream* fringes, a non-dispersive medium yields only an anti-correlation trace for $u_{out} - d2_{out}$ in this region, so features at a non-zero upstream location must be due to the dispersive nature of the Bogoliubov spectrum — as in the simple case studied in [58], where a sinc modulation was observed along a $g^{(2)}(x = cst > 0, x' < 0)$ line in the SE and NW quadrants.

Appendix F: Constraints on the calculations

All configurations in Table I have been realised with the cavity parameters of [11]. When exploring all possible configurations of fluid density on either side of the horizon, some constraints must be abode by.

The first constraint is on the upstream pump wavevector $k_{p,u}$ for a fluid near the sonic point. The fluid is at the sonic

point for

$$c_u = \sqrt{\frac{\omega_p - \omega_0 - \hbar k_{p,u}^2/2m}{m}}, \quad (\text{F1})$$

together with the upstream condition $v_u < c_u$, this yields an upper bound for the upstream fluid flow velocity and thus for the wavevector of the pump:

$$\omega_p - \omega_0 > \frac{3}{2} m v_u^2. \quad (\text{F2})$$

For the value of detuning used throughout this paper the upper bound is around $k_{p,u} = 0.28 \mu\text{m}^{-1}$. In most simulations, we used $k_{p,u} = 0.25 \mu\text{m}^{-1}$ in order to be close to the bound while leaving a small interval for easier simulations.

Exploring all regimes of density in the downstream region comes with some constraints as well: For instance, placing the fluid in the upper part of the bistable regime as in configurations I-4 is easier for a large bistable interval $F_1 - F_2$. Point β in configuration 5 f) is obtained at

$$c_d = \sqrt{\frac{\omega_p - \omega_0 - \hbar k_{p,d}^2/2m}{2m}}. \quad (\text{F3})$$

and the width of the interval is then given by

$$\begin{aligned} \Delta I^{bistable} &= |F_{p,max}|^2 - |F_{p,min}|^2 \\ &= \left[\frac{4}{9} \left(\omega_p - \omega_0 - \frac{\hbar k_{p,d}^2}{2m} \right)^2 - \frac{1}{2} \gamma^2 \right] \times \\ &\quad \frac{\omega_p - \omega_0 - \hbar k_{p,d}^2/2m}{3g}. \end{aligned} \quad (\text{F4})$$

The larger downstream wavevector $k_{p,d}$ results in a larger interval, thus rendering simulation at a wanted point along the bistability loop easier. Nevertheless, a bistable regime exists only if $\omega_p - \omega_0 > \hbar k_{p,d}^2/2m$, hence an upper bound on $k_{p,d}$.

Furthermore, the speed of sound right after the defect, c_{def} is fixed by the upstream parameters and the strength of the defect, V_{def} . Pumping in the upper branch of the bistability requires

$$c_d > \sqrt{\frac{\omega_p - \omega_0 - \hbar k_{p,d}^2/2m}{m}}. \quad (\text{F5})$$

This critical point needs to be below c_{def} for the fluid density to be on the upper branch. Another possibility is to change the value of c_{def} , which can be achieved for a weaker defect potential (energy conservation before and just after the defect links V_{def} and c_{def}), as in configuration I-2. The choice of different $k_{p,d}$ in the simulation given in table I is a consequence of all these constraints.

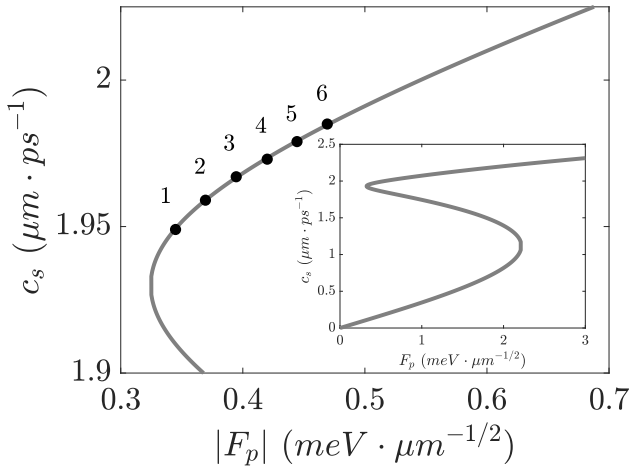
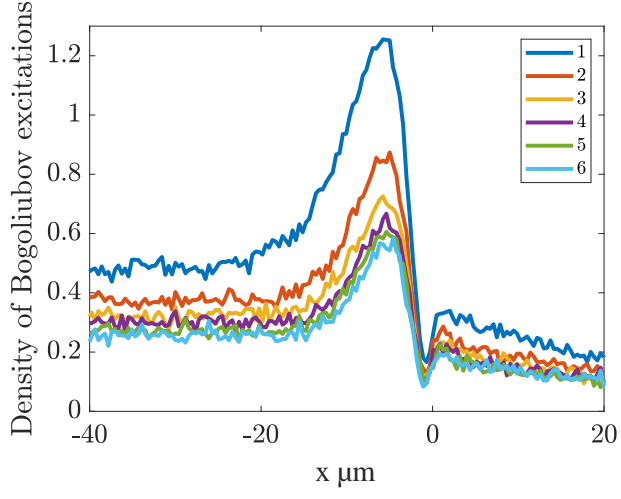


Figure 9. **Density of Bogoliubov excitations in the vicinity of the defect for fluid densities near the sonic point.** **a):** Eq. (D1) for various pump strength with $k_p, u = 0.24 \mu\text{m}^{-1}$. **b):** corresponding fluid densities along the bistability loop.